Nano Scale Disruptive Silicon-Plasmonic Platform for Chip-to-Chip Interconnection

Report on Plasmonic Photodetectors

Deliverable no.:	D 4.5
Due date:	05/6/2015
Actual Submission date:	05/8/2015
Authors:	UVEG
Work package(s):	WP4
Distribution level:	RE[1] (NAVOLCHI Consortium)
Nature:	document, available online in the restricted area of the NAVOLCHI webpage

List of Partners concerned

Partner number	Partner name	Partner short name	Country	Date enter project	Date exit project
5	UNIVERSITAT DE VALENCIA	UVEG	Spain	M1	M45

[1] **PU** = Public
PP = Restricted to other programme participants (including the Commission Services)
RE = Restricted to a group specified by the consortium (including the Commission Services)
CO = Confidential, only for members of the consortium (including the Commission Services)

Deliverable Responsible

Organization: UVEG
Contact Person: Juan P. Martínez Pastor
Address: Instituto de Ciencia de los Materiales, Universidad de Valencia
P.O. Box 22085, 46071 Valencia
Phone: +34963544793
Fax: +34963543633
E-mail: martinep@uv.es

Executive Summary

In the present deliverable most results achieved regarding QD-based photodetectors are summarized. Firstly, the optimized synthesis of PbS QDs for near infrared detection is described, other than more recent activities regarding lead-free QD material, Ag_2Se. Secondly, we give an overview of the preparation of conductive QD-solids from QD colloidal solution by using a very promising large area deposition technique, DrBlading, other than structural and electronic properties of these layers, as obtained from TEM and XPS measurements, in the latter case regarding the effect of ligand exchange and stability of the QD-solid exposed to ambient conditions. Thirdly, we summarize our activities regarding plasmonic structures for integrated photonics, including the design of a plasmonic nanogap photodetector. Finally, we present the fabrication of Schottky-heterostructure photodetectors together with the best electro-optical results obtained on them: peak responsivities of 0.48 and 0.18 A/W at around 1300 and 1500 nm, other than giving the most recent results on the fabrication and characterization of microgap and nanogap photoconductors. In these photodevices the QD-solid is created by dropping and ligand exchange, as the best working method, even if giving rise to layers with a higher granularity and less stable in ambient conditions than in the case of Schottky photodetectors. In spite of these negative features good responsivities are measured under sufficiently high bias voltages.

Change Records

Version	Date	Changes	Author
1	2015-05-1	1st version	Juan Martínez Pastor
2	2015-07-1	revised	Juan Martínez Pastor
3	2015-08-25	revised	Juan Martínez Pastor
4	2015-09-15	updated	Juan Martínez Pastor

1.- Introduction and objectives

A signal generated at the plasmonic transmitter chip (laser plus modulator) has to be measured by a plasmonic receiver in order to be processed electronically. For this purpose, the receiver needs to accomplish the following conditions. Firstly, low-level signals coupled to a plasmonic waveguide (photons are transformed into propagating Surface Plasmon Polaritons -SPPs-) will be amplified before the input of the detector in order to enhance the sensitivity of the receiver. Secondly, the incoming signal in the detector will convert the amplified SPPs into an electrical signal. With the intention to improve the chip-to-chip interconnection integration, amplifier and detector will be designed into the same silicon substrate[1], as it is illustrated in Fig. 1.1

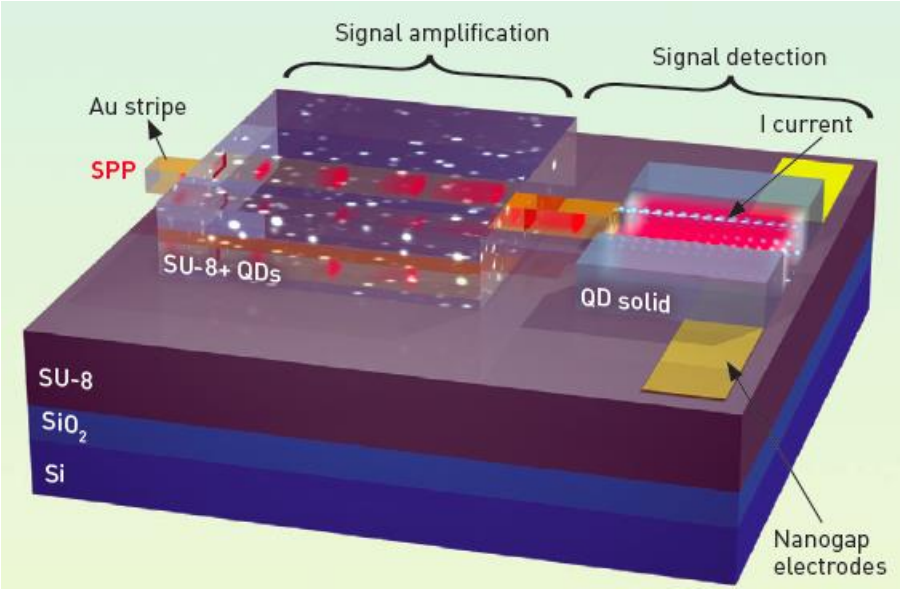

Figure 1: Plasmonic receiver with SPP amplifier and a photodetector. From Ref. 1

The photodetector (on the right of Fig. 1.1) will consist of a conductive layer or integrated Schottky photodiode based on PbS quantum dots (QDs) able to generate an electrical current as a response of the incoming photons[2]. Reported photoconductive responsivities in recent literature are in the range of 0.1-3.9 A/W for a PbS QD monolayer in a nanogap-electrode structure[3], larger than 100 A/W in the case of microgap-electrode structures with PbS layers thicker than 200 nm[4] and more than 10^6 A/W in a MOS microgap-structure based on a PbS layer (60-80 nm thick) on graphene[5]. The QD-solid (conductive layer of QDs) approximation is considered one of the latest advanced concepts for photodetection, given the high absorption of quantum dots, the low cost of the solution processing technique used to deposit the material as well as its integration in Si technology. Furthermore, this concept can be easily combined with plasmonic layers based on metal nanoparticles, because an enhancement of the responsivity is expected due to light trapping effect at the band edge of the QD-solid[4].

To achieve the goals proposed in Navolchi, we need to address:

- Synthesis and characterization of infrared colloidal QDs (PbS and $AgSe_2$ have been developed along the project).
- Preparation and characterization of QD-solids based on PbS and $AgSe_2$ nanocrystals.
- Plasmonic effects for light capture and electric field enhancement.

- Device fabrication and electrical characterization

2.- Synthesis and characterization of infrared colloidal QDs

a. PbS QDs

The synthesis of QDs for IR is based on the hot injection of metal-organic precursors into coordinating/non-coordinating solvents at elevated temperatures. This strategy is established to be the mainstream strategy in the synthesis of high quality semiconductor nanocrystals. The synthesis of PbS (and PbSe) QDs was developed by the spin-off company of the UVEG group. Typically, lead oleate and bis(trimethylsilyl) sulfide (TMS) are used as precursors and fixing a Pb to S precursor ratio to 2:1, which is within the typical range employed in cadmium chalcogenide and lead chalcogenide nanocrystal synthesis[6]. A slow cooling following sulfur precursor injection is employed to obtain narrow size distribution and well-defined excitonic features in absorption and emission spectra, as observed in Fig. 2a.

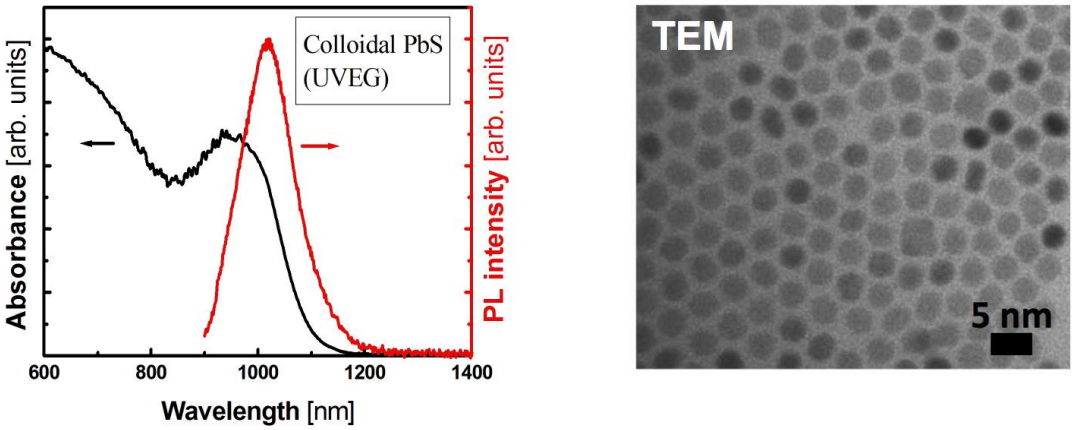

Figure 2: (a) Absorption and PL spectra of as-synthesized PbS colloidal QDs in toluene and (b) TEM image of these PbS QDs.

Figure 2a shows the absorbance spectrum of standard acid oleic-capped PbS colloidal QDs in toluene. As can be observed PbS QDs showed a well-defined absorption excitonic peak centered at around 970 nm. The average size of these QDs is around 3.2 nm (also consistent with TEM images, Fig. 3b), approximately, as calculated from the equation proposed by Moreels *et al.*[7]:

$$E^0 = 0.41 + (0.0252d^2 + 0.283d)^{-1}$$

where E_0 is the effective bandgap (1.30 eV in the case of QDs in Fig. 3) and d is the PbS QD diameter in nm. These PbS QDs were mainly used for developing QD-solid films by the layer-by-layer method in order to compare with most of results published in literature (Refs. 2-5, as some of the most representative). After this initial optimization period, all synthesized PbS QDs, used for creating QD-solids and the fabrication of photodetectors, exhibited excitonic absorption and photoluminescence at infrared telecom wavelengths, as the typical case shown in Fig. 3a. The synthesis developed for these infrared QDs use lead chloride ($PbCl_2$) and elemental sulfur (S) in oleylamine, which simultaneously acts as ligand and solvent. This elemental-sulfur-based

synthesis reported by Cademartiri *et al.*[8] has been optimized to produce large PbS nanocrystals of around 6 – 7 nm in diameter (Fig. 3b). Following this synthetic route we are able to reproducibly obtain monodisperse PbS QDs suspensions emitting at infrared wavelengths, highly air-stable and with high PL quantum yield (QY)[9]. The Pb to S molar ratio was chosen 3:1 to provide QDs with a Pb-rich surface.

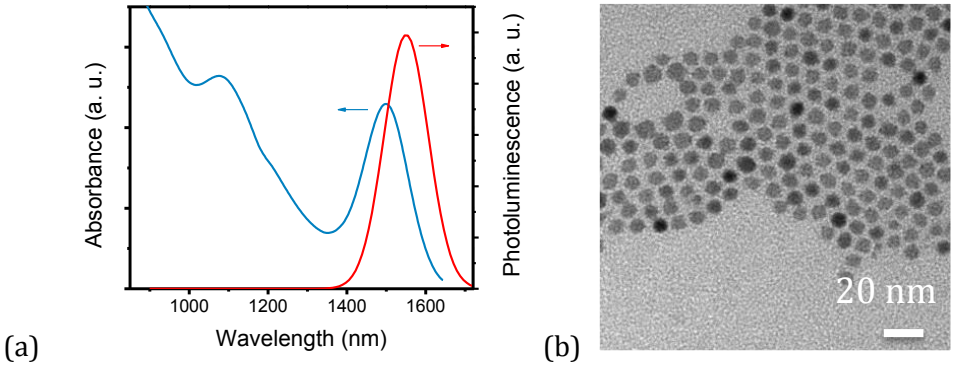

Figure 3: (a) Absorbance (blue line) and photoluminescence (red line) spectra of as-synthesized PbS QDs in octane and (b) TEM image of these PbS QDs.

High-resolution transmission electron microscopy (HRTEM) images (Fig. 4a) suggest that the nanocrystals are highly crystalline and free from stacking faults and lattice defects; from this image a lattice spacing of 0.59 nm is measured along the [001] direction, which is consistent with the rock salt structure of bulk PbS. In PbS QD films the average crystallinity is well observed from X-ray diffraction measurements (Fig. 4b), whose pattern correspond to the rock salt crystal structure of PbS with a lattice constant of 0.5937 nm. The diffraction peaks at 2θ = 26º, 30.1º, 43.1º, 50.9º, 53.4º, and 62.9º perfectly match with (111), (200), (220), (311), (222), and (400) crystalline planes of cubic phase (galena) of bulk PbS (JCPDS Card File No. 5-592).

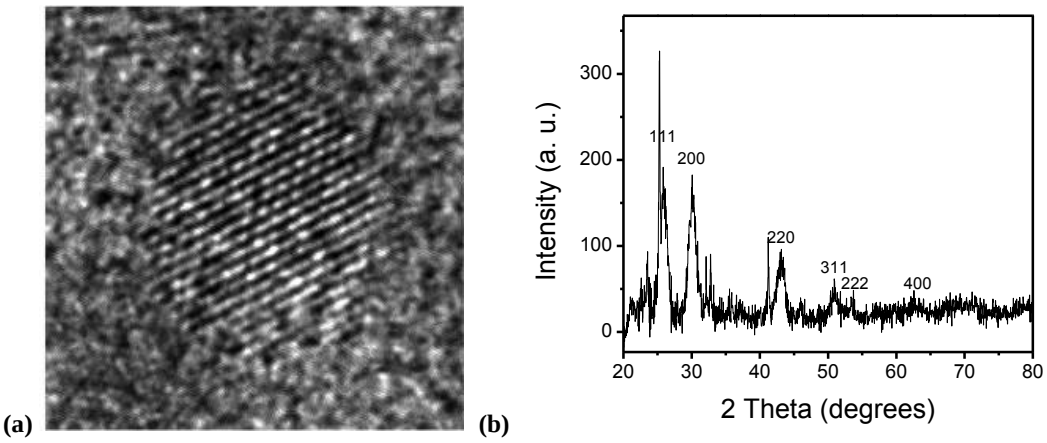

Figure 4: a) HRTEM image of a PbS QD showing crystallinity and absence of lattice defects, (b) X-ray diffraction pattern measured in a compact film of PbS QDs 100 nm thick.

The use of Oleylamine as capping agent to passivate the PbS QDs is necessary to facilitate a

more efficient ligand exchange during the device fabrication. The oleylamine coordinates the surface Pb atoms through the nitrogen lone pair of the amine, which results in a weaker bond than that, for instance, produced by the carboxylic group of the oleic acid. This allows for a faster and more efficient solid-state ligand exchange during device fabrication.

b. $AgSe_2$ QDs

$AgSe_2$ QDs is a lead free alternative to PbS QDs for near infrared optoelectronics. The synthesis and preparation of QD-solids was achieved. Figure 5 shows standard (Fig. 5a) and high resolution (Fig. 5b) TEM images. They exhibit crystalinity, but we observe a large spread in the QD sizes around the average diameter, around 7 nm, thus far from a monodisperse distribution as was observed for PbS (see Fig. 3). Consequently, the PL emission is weak and broad (Fig. 6a), possibly determined by the bigger QDs of the distribution, and absorbance spectra in visible and NIR regions (Figs. 6b-c) do not exhibit any clear excitonic resonance, only an increasing absorbance from infrared to visible wavelengths.

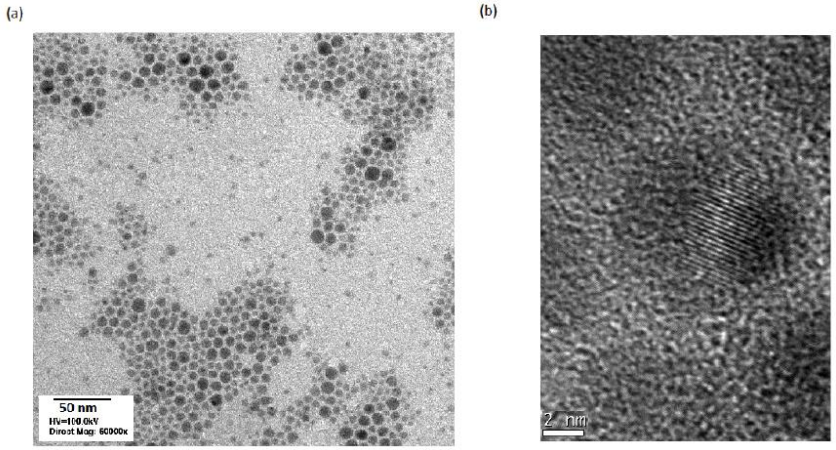

Figure 5: TEM (a) and HRTEM (b) images of $AgSe_2$ QDs

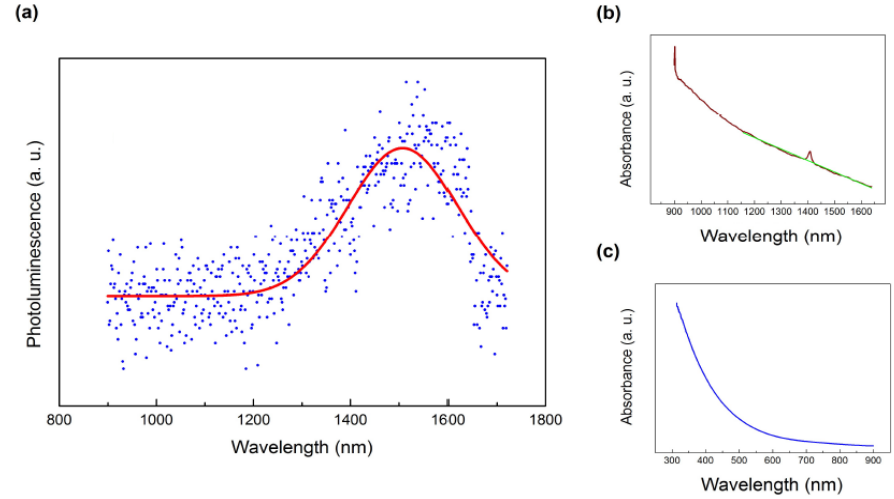

Figure 6: PL (a) and visible (b) / NIR (c) absorbance spectra in a colloidal solution of $AgSe_2$ QDs.

3.- Preparation and characterization of QD-solids based on PbS and $AgSe_2$ nanocrystals

a. PbS QDs

The production of QD-solids is based on a solution-processing method called Layer-by-Layer (LbL) by using spin-coating, which is illustrated in Fig. 7. These QD-solids has been successfully applied in the fabrication of infrared photodetectors and solar cells (see Refs. 2-5 as a good example).

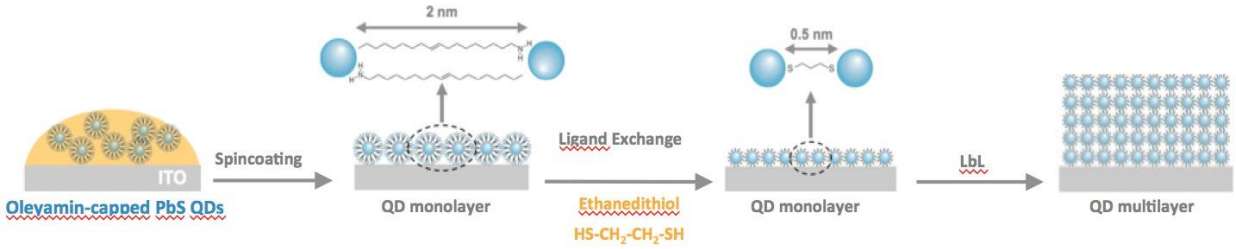

Figure 7: Scheme of the LBL approach.

For further optimization of the PbS QD-solids we employed a layer-by-layer Doctor Blading method for spreading the QD solution on different substrates (glass and glass/ITO/PDOT), which is a novelty in comparison to methods commonly used by other groups. The fabrication protocol consisted on the deposition of the PbS QDs dispersed in octane followed by a bake at 110 ºC for 5 min. This process was repeated seven times to produce a film of 350 nm, for example. The film was then baked at 100 ºC under vacuum for 1 h. Afterwards, the sample was dipped in a solution of MPA in methanol (10 % by volume) for a short time (that has been optimized as explained below) allowing the replacement of the original oleylamine molecules for MPA. Then, the sample was rinsed with methanol to remove the MPA excess, dried under N_2 flow, and annealed again at 100 ºC under vacuum for 1 h. This ligand exchange is the key to produce (a relatively) high mobility QD-solid, given that the initial PbS QD-solid passivated by the original oleylamine ligands used during the synthesis exhibit extremely low mobility as a result of the insulating nature of the long alkyl chains[10]. The replacement by MPA shorter ligands increases the electronic coupling between neighboring QDs and hence the conductivity of the layer[11]. Furthermore, the density and energetic distribution of defects below the conduction band associated to MPA ligands are reduced in comparison to other organic molecules.

XPS measurements were performed to study the surface state of the PbS QD-solid and the chemical effects of the surface QD before and after the ligand exchange process. Figures 8a–c show detailed XPS spectra of the S 2p, Pb 4f and O 1s core levels acquired in samples prepared under different ligand-exchange time conditions. In general terms, several doublets, in the case of the p and f core-levels, and singlets, in the case of the s core-levels, can be deconvoluted from the XPS spectra. The S 2p and Pb 4f XPS spectra of the as-synthesized PbS QDs seem to be dominated by the presence of a doublet whose S 2p3/2 and Pb 4f7/2 appear at 160.9 ± 0.2 and 137.9 ± 0.2 eV, respectively, which are attributed to bulk-like PbS present at the core of the

QDs[12]. This assumption is supported also by the fact that the intensity ratio analysis of these Pb 4f and S 2p components gives a S:Pb ratio of 1.4:1, reasonably close to unity. Besides to signal coming from bulk-like PbS, additional higher energy components with lower intensity can be resolved, which stem from species located at the shell of the QDs[12,13]. With regard to the S 2p spectrum (Fig. 8a), a higher energy component can be identified at ~164.0 eV attributable to S-S bounds, whereas the feature located and ~166.6 eV can be attributed to $PbSO_3$[12,13]. It worths to mention that no traces from other oxidized forms of sulphur, such as $PbSO_4$[13], were detected in the S 2p spectrum of the QDs studied. In the Pb 4f spectrum (Fig. 8b), only a higher energy component has been resolved at ~138.6 eV, which stems from oxidized forms of Pb. The O 1s core level spectrum acquired from PbS QDs with no ligand exchange (Fig. 8c), which is reproduced by using a single component located at 531.0 ± 0.2 eV, may serve us to clarify the nature of the oxidized Pb specie present in these QDs. On one side, previous XPS studies made on PbS QDs have assigned the presence of an O 1s core-level component at ~531 eV to $PbSO_3$[13.14]. On the other side, the intensity ratio analysis between the oxidized Pb 4f core-level component and the O1s peak obtained gives an O:Pb ratio of. 3.4:1. These results indicate that the high energy component observed in the Pb 4f core level measured in PbS QDs mainly comes from $PbSO_3$.

Comparing the XPS results obtained in films prepared in as-synthesized PbS QDs with those obtained after 30 s of ligand exchange process (Figs. 8a–c), it can be seen that chemical composition of the PbS QDs does not seems to change drastically at initial stages of the ligand exchange process, apart from an increase of the relative atomic ratio of oxidized Pb with respect to Pb bound to S (Fig. 8d), that indicates that short ligand exchange process mainly tends to enhance oxidation of Pb atoms at the shell of the QDs. However, deep chemical changes are observed when PbS QDs are exposed to ligand exchange times beyond 60 s. First, the presence of species different from divalent S of PbS appears to be strongly reduced (Fig. 8a). In addition to this, the photoemission peaks composing the S 2p doublet attributed to PbS seem to be better resolved due to a decrease in their full-width at half maximum in a factor ~0.6. With regard to the Pb 4f core-level (Fig. 8b), the relative atomic ratio between oxidized Pb and Pb bound to S appears to continuously increase with the ligand-exchange process time (Fig. 8d). Consistently with this fact, the main peak observed at the O 1s core-level strongly increases with the ligand-exchange process time (Fig. 8c). However, this peak seems to shift by ~0.6 eV to higher binding energies (it is located at 531.6 when the ligand exchange process time is of 120 s) at the same time that two weak features appear to be resolved at both sides of the main O 1s peak. These results indicate that the ligand-exchange process promotes the oxidation of the QD surface and the development of an oxidized shell that strongly reduces the presence of sulphites at the QD shell and collaterally improves the overall structural quality of the remaining bulk-like PbS core.

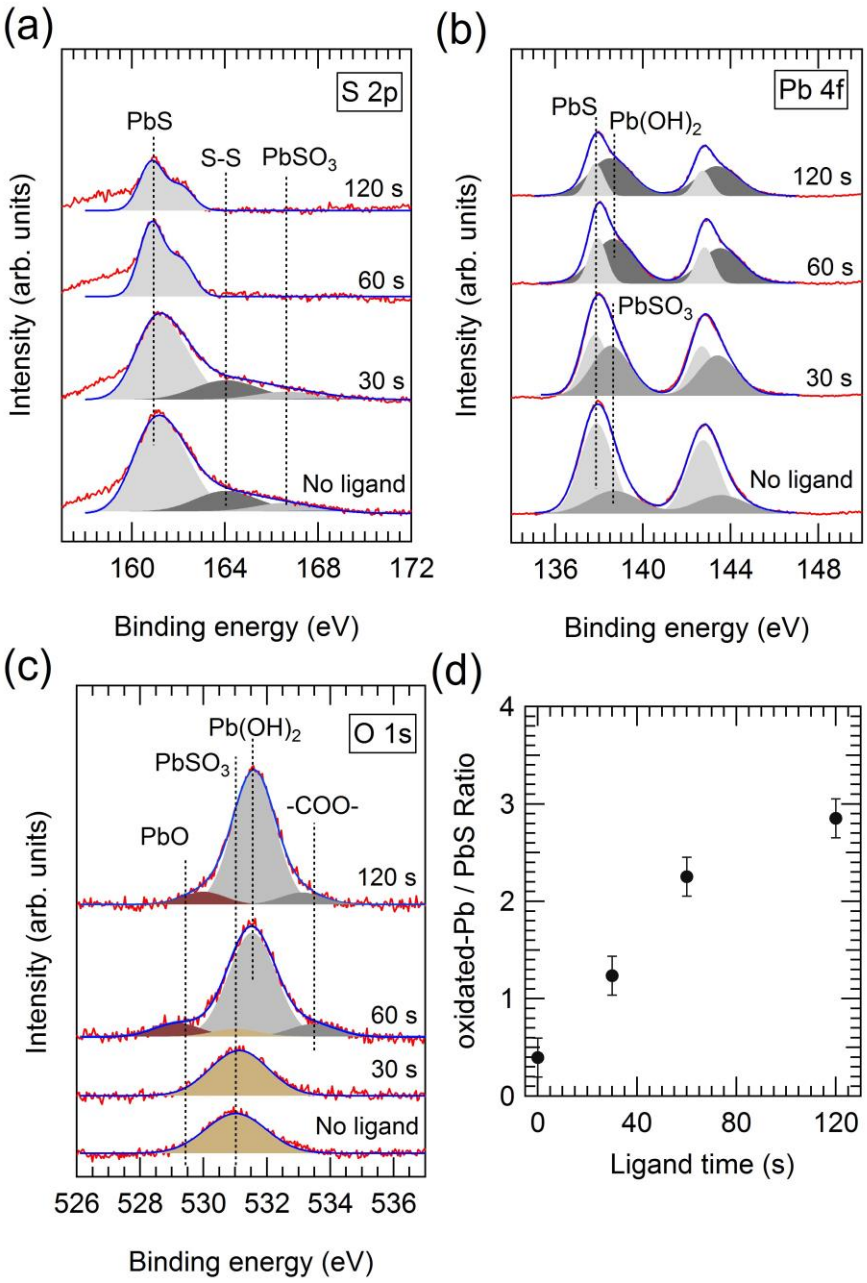

Figure 8: XPS spectra of S 2p (a), Pb 4f (b) and O 1s (c) core levels acquired in samples prepared under different ligand-exchange time conditions, and oxidized-Pb to PbS ratio as a function of ligand exchange time (d).

Our XPS results also can bring some light into the question of the structural composition of the oxidized shell produced after the ligand exchange process. As we have mentioned above, long ligand-exchange process times seem to promote the development of other oxidized species different from $PbSO_3$. The deconvolution of the O 1s peak measured in samples prepared with 60 and 120 s of ligand-exchange process reveals that the $PbSO_3$ component detected in PbS QDs before ligand exchange becomes extremely reduced, simultaneously to the appearance new O 1s component emerging at 531.6 ± 0.2 eV and two weaker signals located at 529.4 ± 0.4 and 533.5 ± 0.2 eV, as observed in Fig. 8c. The first weak peak at 529.4 can be attributed to PbO[13,14] whereas the last weak peak at 533.5 eV seems to come from carboxyl groups of the ligands[12]. The main peak, at 531.6 eV, can be attributed mainly to $Pb(OH)_2$[12]. The assignation of this O 1s peak to $Pb(OH)_2$ suggests that also the high energy Pb 4f component located at ~138.6 eV

mainly comes from $Pb(OH)_2$ after ligand exchange, which is consistent with previous observations[12]. In fact, after aging the samples under ambient conditions in air (Fig. 9), XPS measurements revealed a continuous increasing, with the exposition time in air, of the relative weight of the $Pb(OH)_2$-related components to the whole Pb 4f and O 1s core levels, due to water adsorption. In spite of these evidences, we cannot completely discard that other oxidized species, such as carboxyl groups may also contribute to the main O 1s peak[15]. In fact, the analysis of the XPS intensity ratio between the main O 1s component and the oxidized Pb 4f component yields and effective atomic O-oxidized:Pb-oxidized ratio of the order of 4. However, when the 3 months aged sample is measured by XPS after Ar^+ sputtering in ultrahigh-vacuum (Figs. 10a-c), the effective atomic O-oxidized:Pb-oxidized becomes of the order of ~2, as expected for $Pb(OH)_2$.

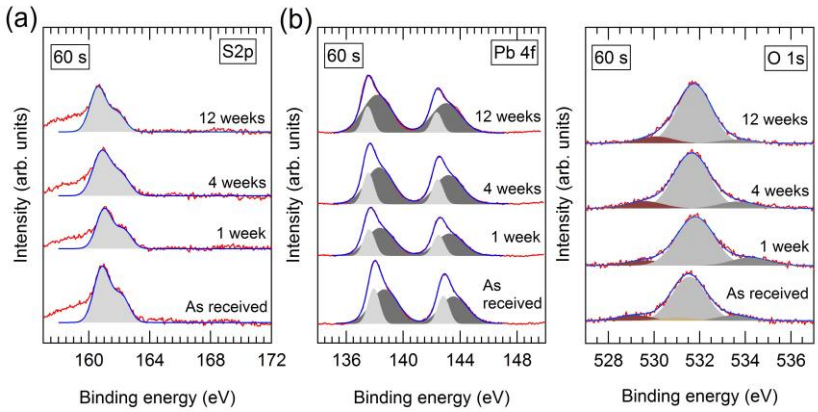

Figure 9: XPS spectra of S 2p (a), Pb 4f (b) and O 1s (c) core levels acquired as a function of aging time.

By XPS, we have detected the presence of Cl in all samples prepared in this work. Figure 8(d) shows a typical Cl 2p core level spectrum measured in one sample prepared after 60 s of ligand exchange and kept in air for 3 months. The observation of this element raises the question about its residual role and the nature of its bonding, if occurs, to the PbS QDs. However, in spite of the observation of a clear Cl 2p core-level peak, no Pb-Cl related component have been clearly resolved in the measured Pb 4f spectra, at energies expected around 139 eV[16]. At first sight, this fact may imply that Cl is a residual product of the PbS preparation. However, the behavior of the Cl 2p peak after Ar^+ sputtering (Fig. 10d) suggests that Cl-Pb bonding would take place, given that Ar^+ sputtering should enhance the signal from the PbS QD core and even break the existing Pb-S and Pb-O bonds, but, what is relevant here, is the observation that all core-levels related to PbS QDs shift by 0.4 eV to higher binding energies, which can be originated by a QD size reduction inherent to the sputtering process (of course, the C 1s binding energy from residual C remains at 285 eV (not shown))[17]. As all the PbS-related core levels do, the Cl 2p core level appears also to shift to higher binding energies, which indicates that these Cl are linked to PbS QDs, probably as PbCl2. It should be remarked here that, although this working frame suggests that ligand exchange process improves the structural quality of the remaining PbS QD core, also increases the overall size of the oxidized shell of the PbS QD. These facts should be taken into account in view of optoelectronic applications of PbS QDs. The stability of QDs is relevant in view of their optoelectronic applications too. This issue has been approached here through the study by XPS of samples kept in air for even three months (Fig. 9). Besides the water absorption process mentioned above, we can notice that the Pb 4f and S 2p core level components attributed to PbS did not evidence any change in width, which indicates that QDs shell effectively passivates the surface and protects the bulklike PbS core.

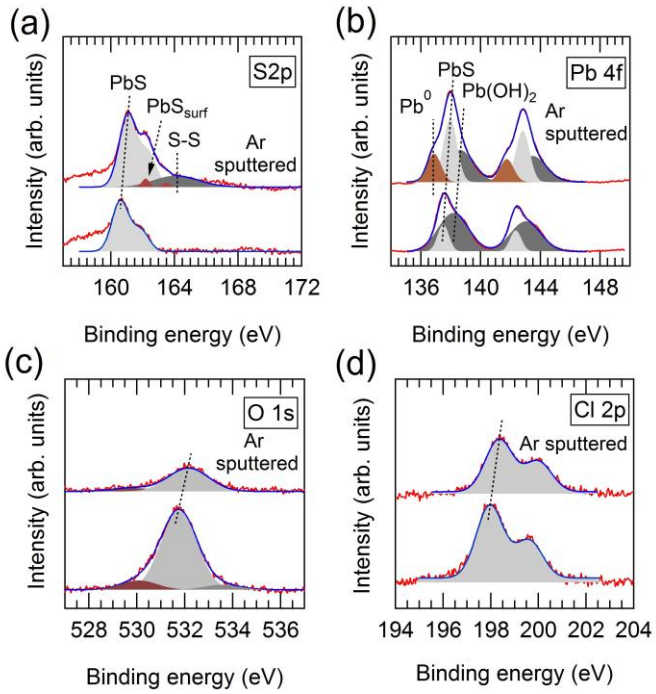

Figure 10: XPS spectra of S 2p (a), Pb 4f (b), O 1s (c) and Cl 2p (d) core levels acquired before and after Ar sputtering.

Regarding optical properties of these PbS QD-solids, the PL band and absorption band-edge spectra are very similar to those obtained in the colloid (Fig. 3a). Finally, the electrical properties of the PbS QD-solids films with completed ligand exchange are characterized by a high resistivity around 10^5 Ωcm, a hole concentration larger than 10^{15} cm^{-3} and mobilities smaller than 0.065 cm^2/Vs, as estimated from Hall measurements (very difficult to carry out due to the extremely high resistivity).

b. $AgSe_2$ QDs

$AgSe_2$ QD-solids have been also prepared by the same LBL method after DrBlading deposition of the colloidal solution. The resistivity is much lower (three orders of magnitude, approximately) than that obtained in PbS QD-solids, which is translated in a larger dark current in micro-photoconductors. This is possibly due to a more important background doping of these QD-MPA hybrid solid, because one would expect less important electronic coupling between QDs of very different sizes (from 5 to 10 nm, as was noted in Fig. 5a). In fact, this should be the reason why the measured photocurrents are very low as compared to PbS photoconductors (not shown here), given the increasing importance of trapping and recombination of carriers in the biggest QDs. In spite of the low measured photocurrents our results are better than those available in literature. Therefore, much effort will be paid in next future to improve the synthesis methods to reduce the size dispersion of $AgSe_2$ QDs.

4.- Plasmonic effects for light capture and electric field enhancement

Conducting polymers (CPs) offer a unique combination of electric, electronic and optical properties inherent to semiconductors and metals, with the added value of processability. New multifunctional polymeric materials, which can combine electrical conductivity and photoconductivity with other important properties, such as UV lithographic capabilities, was presented in Deliverable 4.2. More important was the development of metallic nano/microstructures by a chemical regrowth of metal nanoparticles (NPs) used as seeds, which was the base of a patent presented at the end of 2012[18]. The process consisted of three simple steps: (1) fabrication of macro-/micro-/nano-patterns by means of lithography (UV, ebeam) or any other direct printing technologies (inkjet, microplotter, ...), (2) in-situ synthesis of metal NPs during a post-bake step and (3) wet chemistry (non-electrochemical) metallization of nanocomposite patterns. Metal NPs are embedded into the polymer pattern and act as seeds for the reduction of Ag(I) when immersed into a solution of the corresponding precursor metal salt ($AgNO_3$) and an appropriate reducing agent. As a result, metal NPs grow significantly into the nanocomposite structure until the desired final size or until the pattern is completely metallized (see Deliverable 4.2 for more details of the method), as shown in Fig. 11 for nanorods patterned on a glass substrate by using a PVA resist containing the precursor of Ag NPs (step 1) and subjected to different regrowth times (step 3) after step 2. These nanostructures can be used for solid-state plasmonic sensors or the fabrication of metallic waveguides, among other applications.

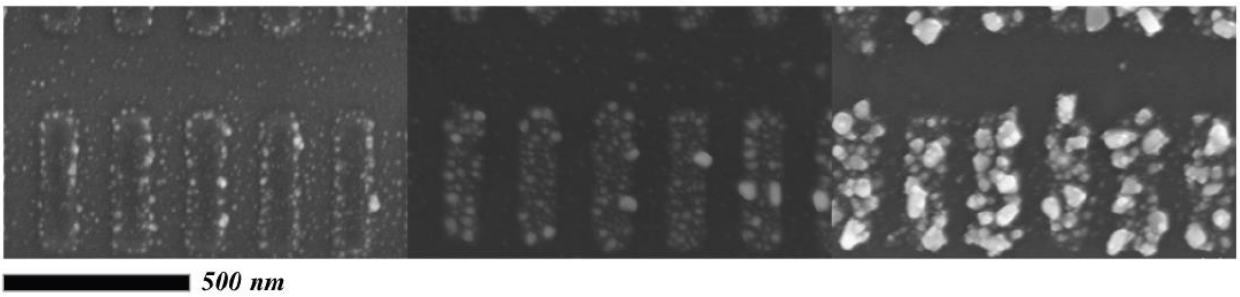

Figure 11: SEM micrographs of patterned nanorods on a glass

More recently, this method have been used to developed new plasmonic couplers based on the incorporation of metal NPs in polymer waveguides fabricated on a Si/SiO_2 substrate[19]. The interaction of light with metal NPs was attracted much interest in recent years because they exhibit unusual optical properties derived from their localized surface plasmon resonance. In particular, high scattering cross sections of these nanostructures can be exploited in the redirection of light into integrated photonics, because it will be useful for light coupling or interaction with active emitters. For this reason, we proposed the incorporation of these nanostructures into the commercially available resist Novolak, in order to provide a suitable technology to define patterns by UV-photolithography. Moreover, the technology allows the control of size of metal NPs in the polymer via the regrowth method explained above, and hence, it becomes possible to tune the plasmonic resonance or to engineer the effective refractive index of the nanocomposite by two degrees of freedom: the size of metal NPs and their density in the pattern b changing the concentration of the metal precursor. We paid special attention to

optimize the fabrication conditions and to study the optical properties of the nanocomposite with the intention to design optical couplers integrated in PMMA waveguides. As a result, by measuring directly light at the output face of the waveguide we demonstrate the coupling in a broad wavelength range (400-780 nm) by illuminating a waveguide from its normal surface, as shown in Fig. 12. This simple coupling method allows efficiencies of 1 % (Fig. 12a), which is in the same order of magnitude as the values obtained by standard techniques established to couple light in optical waveguides (end fire coupling, gratings or prisms).

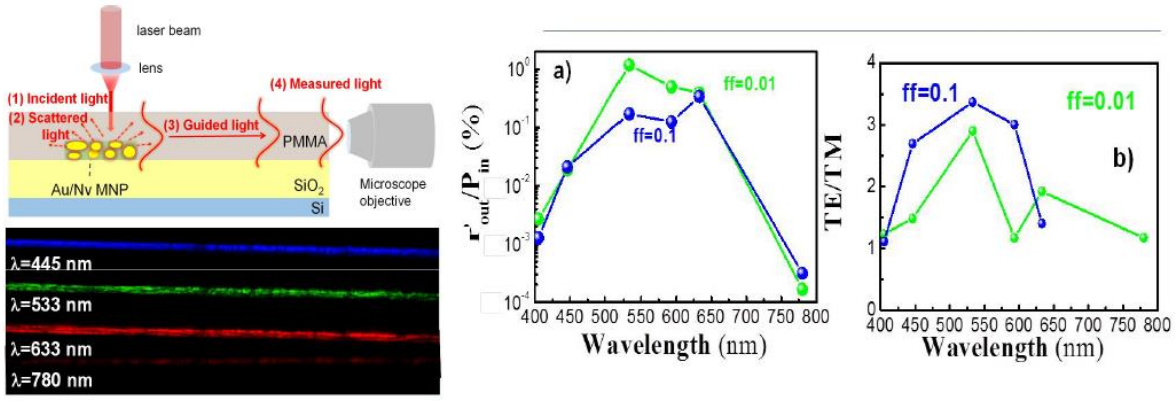

Figure 12: At the left (top) it is shown the scheme of light coupling into a PMMA waveguide through light scattering by metal NPs; the waveguided light at different wavelengths is measured at the leaving face of the waveguide (bottom images). The coupling efficiency and the ratio between TE and TM light at the output of the waveguide as a function of the wavelength is depicted in plots (a) and (b), respectively, at the right side of the figure.

Finally, photodetectors incorporating a plasmonic enhancement (electric field concentration) may be achieved by the particular design of the electrodes using:

(i) nanogap in a nanoantena-like plasmonic structure or
(ii) nanogap plasmonic waveguide structure

In the first case (Fig. 13a) the advantage is the high electric field concentration (leading to an plasmonic absorption enhancement), if the nanogap is sufficiently small, but a very small detection area. In the second case (Fig. 13b) a short nanogap distance can also determine a relatively high plasmonic absorption enhancement (the shortest nanogap value will be limited by fabrication), other than having the advantage of a large detection area, as determined by the desired photodetector footprint. Here the electrodes, which are parallel to the nanogap slit, will have a length in the range from 2 to 5 μm in order to absorb sufficient light coming from the plasmonic amplifier.

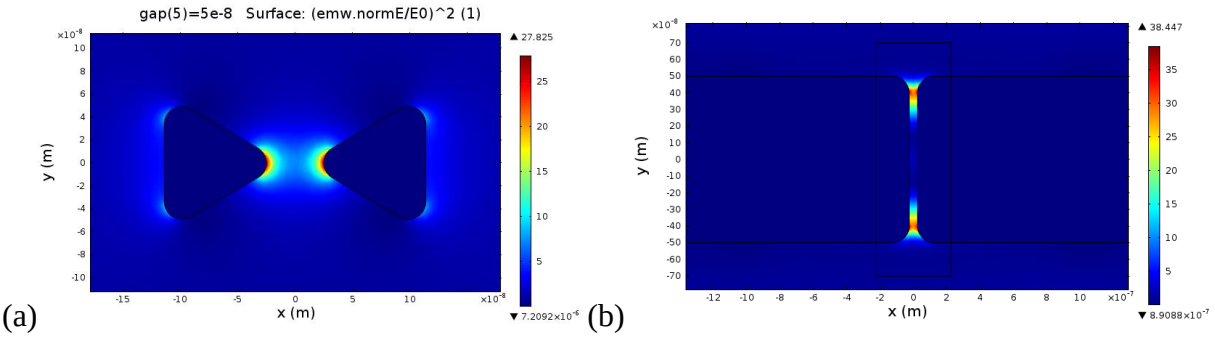

Figure 13: Distribution of electric field intensity at 1550 nm in a bowtie nanoantenna wit a gap distance of 50 nm (a) and in a nano-GPW 1 □m long and the same gap separation (b).

5.- Device fabrication and electrical characterization

a. Schottky-heterostructure photodiodes

In the case of the most recent generation of devices we have obtained peak responsivities of 0.48 and 0.18 A/W at around 1300 and 1500 nm (blue and green lines in Fig. 13). The time response of these photodiodes working in photocurrent mode is estimated to be around 100 □s, very similar to values reported in literature. The photovoltage noise was measured to be of the order of 85 nV/Hz$^{1/2}$ at 1 kHz for the photodiode based in the 500 nm thick PbS QD film, whereas the photocurrent was perfectly linear over more than three orders of magnitude (constant responsivity). The experimental detectivity is estimated to be in the range 10^{12} - 10^{13} Jones. These photodiodes, even if not made with an optimized architecture to be used as a solar cell, when illuminated under AM1 solar conditions, open circuit voltages (V_{oc}) of 200-300 mV were measured in the best photodiodes of the examined generations and short circuit currents (J_{sc}) as high as 10-20 A/cm^2, respectively, which are also in the range of the best expected and reported values using PbS QDs of smaller size as the base for solar cell structures. It is also worth noting that photodiodes fabricated without encapsulation are stable in air during several weeks, even if electrical parameters degrade progressively (after one month in air the responsivity decreased a factor two), possibly due to the protecting effect of the top metal electrode (Ag). More recently, ZnO top electrodes based on conductive nanoparticles, as suggested by other authors[20], have been developed with a relative success in the rectifying I(V) characteristics of the Schottky-heterostructure photodetector, but exhibiting lower photocurrents, possibly due to an increase of the carrier recombination velocity at the PbS-ZnO interface; on the other hand, a very high process temperature (500 ºC) is needed to obtain a sufficiently high conductive layer, even if worse than sputtered layers. Therefore, further investigation is needed prior to the use of these ZnO layers deposited by solution processing technique as electrodes for Schottky-heterostructure photodetectors.

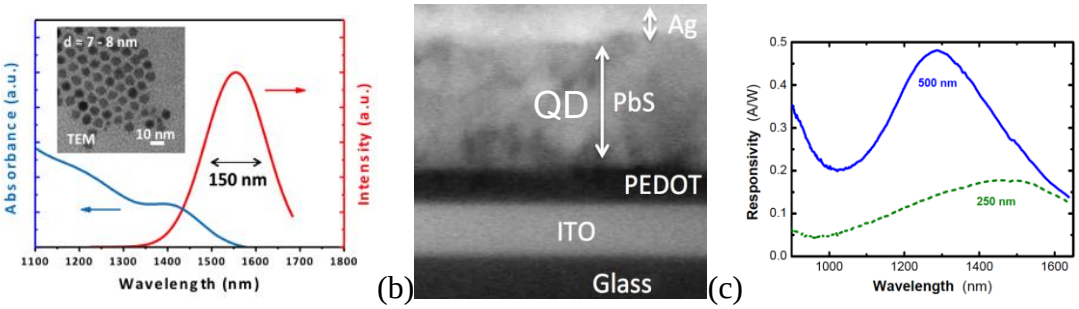

Figure 14: (a) PL (red curve) and absorbance (blue curve) of PbS QDs optimized for photodetectors working at telecom wavelengths; in the inset a TEM image is shown with indication of the QD diameter. (b) Transversal SEM image of a complete Schottky photodiode. (c) Responsivity measured in the best fabricated photodiodes using the same PbS QDs to deposit 250 (green dashed line) and 500 nm (blue continuous line) thick films.

b. QD-solid based microgap/nanogap photoconductors

The Schottky concept is a very convenient device to be integrated in SOI technology, because photocurrent or photovoltage can be directly measured without needing of polarization or used as input for a transimpedance amplifier. However, microgap and nanogap photoconductive devices would offer the most ideal geometry to be integrated in a planar geometry of the final plasmonic chip targeted in NAVOLCHI, other than smaller footprints, faster time response and the possibility to add plasmonic effects in the case of the nanogap photoconductor. Within this task we have developed several series of microgap and interdigitated electrodes (Figs. 15a-b, respectively), whose results are discussed below. In the case of nanogap devices two series have been developed until now, a first one using a very ITO-layer (to produce a better focusing during ebeam patterning) on a quartz substrate and a second one using a Si/SiO_2 substrate with a more complicated layout of fabrication (Figure 15c shows the sample containing 65 nanogap devices); these devices are under current investigation.

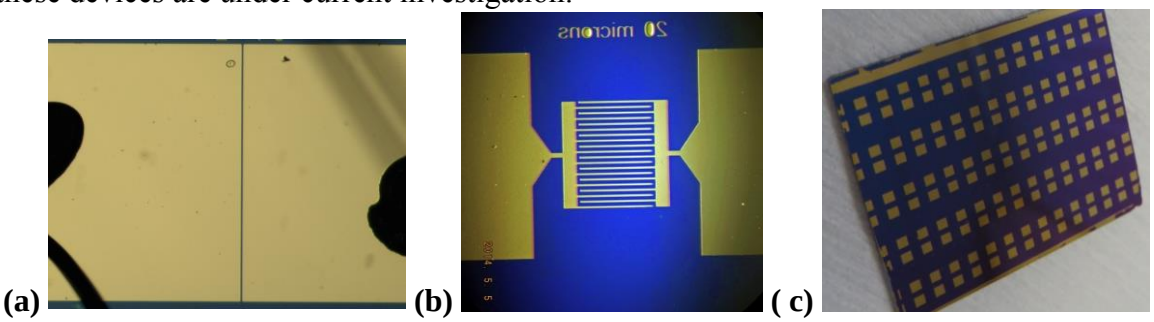

Figure 15: Photographs of single microgap (10 μm gap) (a) and interdigitated (20 μm gap) (a),photoconductors and processed piece of wafer with 1x1 mm^2 pads containing waveguide-nanogap (50-150 nm gaps) devices (c).

As a starting point we fabricated photoconductive devices (200 μm gap) by depositing Ag electrodes on top of a DrBlading film (500 nm thick) with ligand exchange procedure (similarly to the case of Schottky photodiodes) on a glass substrate. For these photoconductors we arrive to photocurrents ≈ 30-50 nA (responsivities very close to 0.1 A/W) in the wavelength range 1200-1500 nm at 200 V bias, despite the big distance between electrodes, over a reasonably low dark current (49 nA).

In the case of single microgap and interdigitated photoconductors the electrodes are patterned on the Si/SiO_2 wafer and created by using lift-off processing. For this reason the QD-solid films should be created in a subsequent step by dropping the QD solution, previous to the ligand exchange procedure and curing. This method is not ideal, because the reduced control of the QD-solid thickness and the formation of important granularity. Another technique that is being optimized is the controlled dispensation of the QD solution by using a microplotter, because it should be the optimal method to create a QD-film on nanogap devices.

The results obtained on the best microgap-based photoconductors are summarized in Fig. 16. Figure 16a shows the photocurrent as a function of the applied bias recorded under solar-AM1 illumination (the incident power is 100 mW/cm^2, giving different collected light in the three devices because of their different active area: 200 and 20 - 10 μW in the interdigitated and 20 - 10 μm gap photoconductors, respectively). The poorest results are observed is the interdigitated photoconductor, possibly due to the inhomogeneity in the QD-film over it largest active area as compared to the case of single microgap photoconductors; on the contrary the interdigitated device would offer the possibility to work with smaller applied bias, given the high number of fingers. For the best device, the 10 μm gap photoconductor, for which we measure a photocurrent around 40 nA at 1300 nm under a bias of 100 V (Fig. 16b), which is translated in a

responsivity of around 1.6 A/W. It is important to mention that microgap devices degrade faster with exposure to ambient than Schottky photodiodes, possibly due to the protecting effect in the latter case due to the top Ag-electrode. For this reason an encapsulation of photoconductor devices has been perfomed after the final ligand exchange and curing processing.

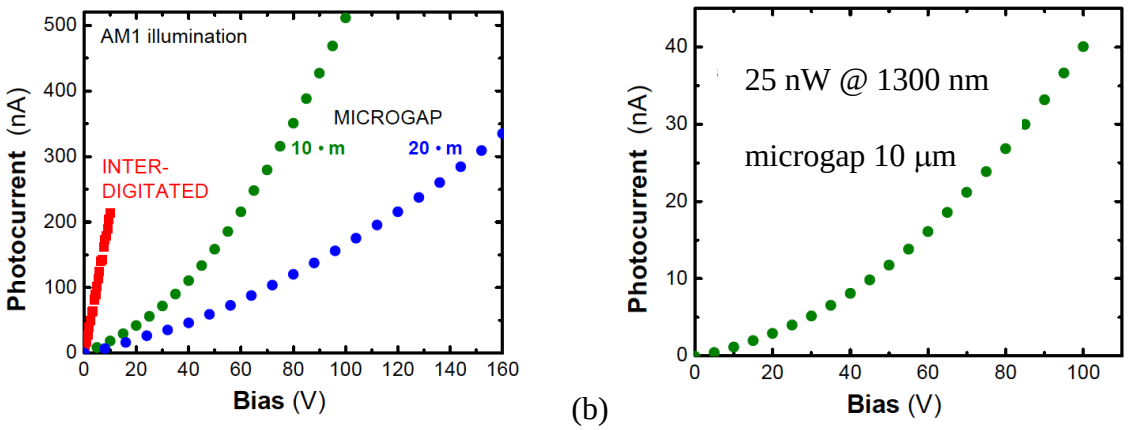

Figure 16: (a) Photocurrent measured in a 20 µm gap interdigitated device (red symbols) as compared to 10 (green symbols) and 20 (blue symbols) µm gap photoconductors as a function of applied bias under AM1-solar illumination. (b) Photocurrent measured in a single microgap (10 µm gap) photoconductor as a function of applied bias under illumination at 1300 nm (25 nW of estimated incident power).

Finally, it is important to note that microgap photoconductors have a more important responsivity for lower incident powers, as shown in Fig. 17 for a 20 µm gap photoconductor after encapsulation, decreasing by near two orders of magnitude from 20 nW to 7 µW of incident power. The measured responsivity at 1500 nm is around 0.14 and 1 A/W under 15 and 30 V bias, being the dark current around 12 and 18 nA, respectively. For a 2 µm gap photoconductor the observed phenomenology is similar, with a responsivity around 0.7 A/W under 2 nW illumination, even if the responsivity stabilizes at 0.02 A/W above 100 nW, that is, the photocurrent does not saturate with power, contrary to the case of the 20 µm gap photoconductor in the examined bias range.

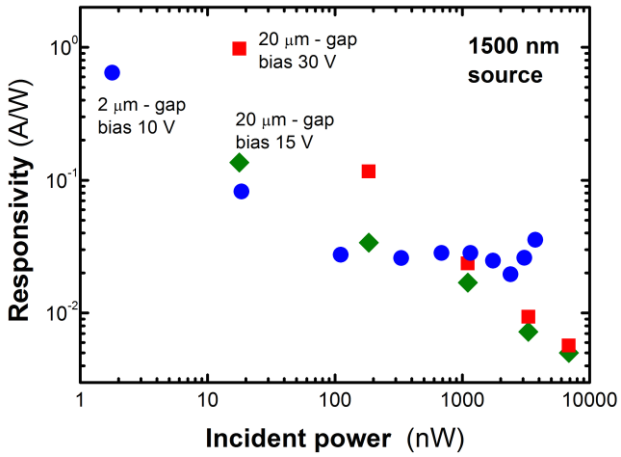

Figure 17: Responsivity measured in a 20 µm gap photoconductor device at several applied bias as a function of the incident power using a 1500 nm laser source, where the PL of PbS QDs is observed after their synthesis.

Plasmonic effects are expected if the distance between electrodes in a gap-waveguide photoconductor (metal-insulator-metal) is smaller than 100 nm: coupling of light both under normal and in-plane incidence and enhancement of the electric field in the nanogap region. The

fabrication of these photoconductor devices (Fig. 18a) on Si-SiO_2 is not simple, because involving several processing steps to define the millimeter size gold pads, micrometer size (from 0.5 to 2 μm) aluminum electrodes and the opened nanogap on them by using RIE after an ebeam patterning on PMMA (Fig. 18b). The preparation and characterization of these devices are under way.

(a) 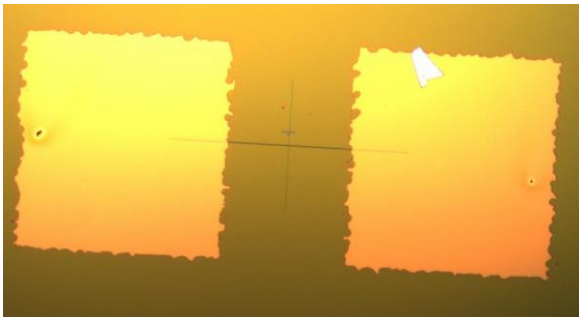 (b) 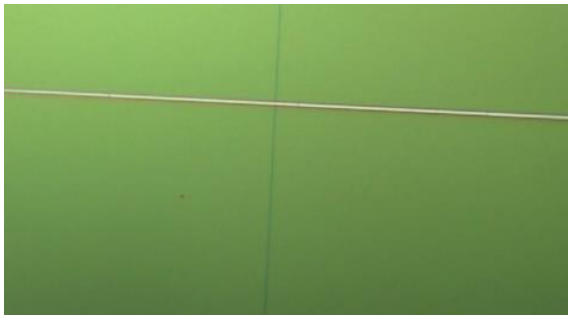

Figure 18: (a) Nanogap devices fabricated on a Si-SiO_2 substrate, (b) detail of fabrication showing the patterned nanogap in the PMMA resist prior to RIE.

6.-Conclusions and outlook

In the present deliverable most results achieved regarding QD-based photodetectors are summarized:

- optimized synthesis of PbS QDs for near infrared detection capped with oleyamine to achieve a successful ligand exchange with MPA,
- lead-free QD material, Ag_2Se, is promising for developing near infrared photodetectors, but its synthesis needs further investigation to reduce the still very broad size dispersion,
- the preparation of high quality conductive QD-solids from QD colloidal solution was achieved by using a very promising large area deposition technique, DrBlading,
- a study of structural and electronic properties of QD-solids was accomplished by means of TEM, X-ray diffraction and XPS measurements (in this case to study the effect of ligand exchange and stability of the QD-solid exposed to ambient conditions),
- the use of our multifunctional polymers to fabricate plasmonic nanostructures with applications in sensing and integrated photonics,
- the design of a plasmonic nanogap photodetector
- peak responsivities of 0.48 and 0.18 A/W at around 1300 and 1500 nm were achieved in Schottky-heterostructure photodetectors,
- successful fabrication of microgap and nanogap photoconductors,
- in the best microgap photoconductors, 2 and 20 μm separation, responsivities of around 0.7 and 1 A/W were measured at 1500 nm under a 10 and 30 V bias, at very low incident powers, respectively.

As an outlook, the results attained in PbS QD-solids and Schottky photodiodes based on them have been presented in several national and international conferences[21] and a paper is being prepared to submit in brief for publication, similarly to the case of microgap photoconductors based on Ag_2Se QDs were advances over literature data were achieved. We have been working on the best conditions to obtain reproducible results in microgap photoconductors that was difficult to be achieved due to granularity and poor stability of the

QD layer obtained by dropping; last generation of microgap photoconductors were encapsulated before characterization to solve stability problems. The formation of similar layers onto nanogap photoconductors and their electro-optical characterization are under current work.

[1] J. Leuthold, S. Muehlbrandt, A. Melikyan, M. Kohl, C. Koos, W. Freude, V. Dolores- Calzadilla, M. Smit, I. Suarez, J. Martínez-Pastor, E.P. Fitrakis and I. Tomkos, "Plasmonic Communications: Light on a Wire", Optics & Photonics News, vol. May 2013, 30-35 (2013).
[2] G. Konstantatos and E.H. Sargent, "Nanostructured materials for photodetection", Nature Nanotechnology **5**, 391-400 (2010).
[3] Ferry Prins, *et al.*: "Fast and Efficient Photodetection in Nanoscale Quantum-Dot Junctions", Nanoletters **12**, 5740–5743 (2012).
[4] F. Pelayo García de Arquer *et al.*, "Plasmonic light trapping leads to responsivity increase in colloidal quantum dot photodetectors", Appl. Phys. Lett. **100**, 043101 (2012).
[5] G. Konstantatos *et al.*, "Hybrid graphene–quantum dot phototransistors with ultrahigh gain", Nature Nanotechnology **7**, 363-368 (2012).
[6] J. E. Murphy, M. C. Beard, A. G. Norman, S. P. Ahrenkiel, J. C. Johnson, P. R. Yu, O. I. Micic, R. J. Ellingson, and A. J. Nozik, J. Am. Chem. Soc. **128**, 3241–3247 (2006).
[7] I. Moreels, K. Lambert, D. Smeets, D. D. Muynck, T. Nollet, J. C. Martins, F. Vanhaecke, A. Vantomme, C. Delerue, G. Allan, Z. Hens, ACS Nano **3**, 3023 (2009).
[8] L. Cademartiri, J. Bertolotti, R. Sapienza, D. S. Wiersma, G. von Freymann, and G. A. Ozin, Multigram Scale, "Solventless, and Diffusion-Controlled Route to Highly Monodisperse PbS Nanocrystals", J. Phys. Chem. B **110**, 671 (2006).
[9] J. Tang, L. Brzozowski, D. Aaron R. Barkhouse, X. Wang, R. Debnath, R. Wolowiec, E. Palmiano, L, Levina, A. G. Pattantyus-Abraham, D. Jamakosmanovic, and Edward H. Sargent, "Quantum Dot Photovoltaics in the Extreme Quantum Confinement Regime: The Surface-Chemical Origins of Exceptional Air- and Light-Stability", ACS Nano **4**, 869 (2010).
[10] D. V. Talapin and C. B. Murray, "PbSe Nanocrystal solids for n- and p-Channel Thin Film Field-Effect Transistors", Science **310**, 86 (2005).
[11] D. V. Talapin, J.-S. Lee, M. V. Kovalenko, and E. V. Shevchenko, "Prospects of colloidal nanocrystals for electronic and optolectronic applications", Chem. Rev. **110**, 389 (2010).
[12] V. Malgras, A. Nattestad, Y. Yamauchi, S. Xue Dou, and J, Ho Kim, "The effect of surface passivation on the structure of sulphur-rich PbS colloidal quantum dots for photovoltaic application", Nanoscale **7**, 5706 (2015).
[13] Ni Zhao, T. P. Osedach, L.-Yi Chang, S. M. Geyer, D. Wanger, M. T. Binda, A. C. Arango, M. G. Bawendi, and V. Bulovic, "Colloidal PbS Quantum Dot Solar Cells with High Fill Factor", *ACS Nano* **4**, 3743 (2010).
[14] E. J. D. Klem, H. Shukla, S. Hinds, D. D. MacNeil, L. Levina, and E. H. Sargent, "Impact of dithiol treatment and air annealing on the conductivity, mobility, and hole density in PbS colloidal quantum dot solids", Appl. Phys. Lett. **92**, 212105 (2008).
[15] D. Zherebetskyy, M. Scheele, Y. Zhang, N. Bronstein, C. Thompson, D. Britt, M. Salmeron, P. Alivisatos, and L.-W. Wang, Science **344**, 1380 (2014).
[16] L. R. Pederson, J. Electron Spectrosc. Relat. Phenom. **28**, 203 (1982).
[17] R. Reiche, R. Thielsch, S. Oswald, and K. Wetzig, J. Electron Spectrosc. Relat. Phenom. **104** 161 (1999).
[18] R. Abargues, P. Cantó Rodríguez, M. L. Martínez Marco, J. Martínez Pastor, and J. L. Valdés, "Method to obtain metallic structures of nano- and micro-metric size from lithographic resists based on nanocomposites", Application No. P201201282, Spain, 28/12/2012, Owners: University of Valencia (50 %), Intenanomat SL (50 %).
[19] M. Signoretto, I. Suárez, V.S. Chirvony, R. Abargues, P.J. Rodríguez-Cantó and J. Martínez-Pastor, "Organic waveguide couplers based on metal nanoparticle-polymer nanocomposites", Nanotechnology, accepted.
[20] B. N. Pal, I. Robel, A. Mohite, R. Laocharoensuk, D. J. Werder, and V. I. Klimov, "High-Sensitivity p–n Junction Photodiodes Based on PbS Nanocrystal Quantum Dots", Adv. Funct. Mater. **22**, 1741 (2012).
[21] A. Maulu, P. J. Rodríguez-Cantó and J. P. Martínez-Pastor, *Colloidal QD-solid photodetectors produced by doctor-blading based on two configurations: nano-gap (MIM) vs Schottky/heterostructure*, 8th International Conference on Quantum Dots, 11-16 May 2014, Pisa (Italy), Oral; A. Maulu, P.J. Rodríguez-Cantó, I. Suarez, R. Abargues, J.P. Martinez-Pastor, *Fabrication of solution-processed QD-solids by doctor blading technique and their application for photodetection*, 4th International Colloids Conference, 15-18 June 2014, Madrid (Spain), Poster; A. Maulu, P. J. RodríGuez-Cantó, J. P. Martínez Pastor, *Efficient photodetectors at telecom wavelengths based on thin films of lead sulfide quantum dots*, Nanomeeting 2015, 26-29 May 2015, Minsk (Belarus), oral contribution. PUBLISHED IN "Physics, Chemistry and Application of Nanostructures (Proceedings of International Conference Nanomeeting – 2015)", World Scientific Pub. Co., ISBN 978-981-4696-51-7, pp. 556-559, 2015; A. Maulu, P. Javier Rodríguez Cantó, J. Navarro Arenas, R. Abargues and J. Martínez Pastor, *Photodetectors at 1.3-1.7 μm Based on Thin Films of PbS Quantum Dots*, IX Reunión Española de Optoelectrónica (IX Spanish Meeting of Optoelectronics), OPTOEL2015, Salamanca (Spain), 13-15 July 2015, Poster.